ACS APPLIED MATERIALS & INTERFACES

Research Article

www.acsami.org

Inorganic–Organic Thiol–ene Coated Mesh for Oil/Water Separation

Qiyi Chen, Al de Leon, and Rigoberto C. Advincula*

Department of Macromolecular Science and Engineering, Case Western Reserve University, Cleveland, Ohio 44106, United States

Supporting Information

ABSTRACT: A highly efficient mesh for oil/water separation was fabricated by using a superhydrophobic and superoleophilic coating of thiol–ene hybrid, consisting of pentaerythritol tetra(3-mercaptopropionate) (PETMP), 2,4,6,8-tetramethyl-2,4,6,8-tetravinylcyclotetrasiloxane (TMTVSi), and hydrophobic fumed silica nanoparticles, via a simple two-step fabrication process. Spray deposition and UV curing photopolymerization were sequentially performed, during which solvent evaporation provides microscale roughness while nanoparticle aggregation forms nanoscale roughness. The hierarchical morphologies were stabilized after UV curing photopolymerization. High contact angle (>150°) and low roll-off angle (<5°) were achieved due to the multiscale roughness structure of the hierarchical morphologies. These coatings also have excellent chemical resistance, as well as temperature and pH stability, after curing.

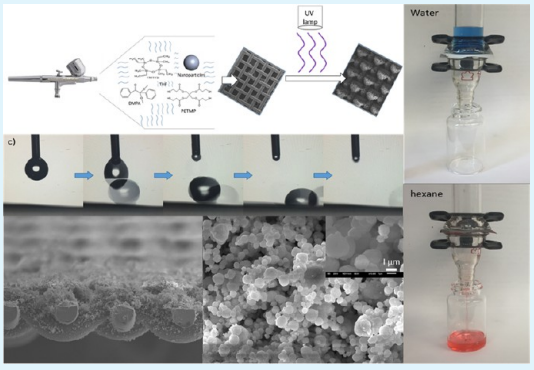

KEYWORDS: *thiol–ene chemistry, superhydrophobic, superoleophilic, oil/water separation, spray-coating, UV-curing, silica nanoparticles*

INTRODUCTION

Superhydrophobicity, defined as a contact angle higher than 150° and a roll-off angle smaller than 10°, was first discovered from the surface of lotus leaves,[1−3] where it was observed that water can roll around without wetting the surface. Since then, superhydrophobicity has gained plenty of interest from many researchers. The Cassie–Baxter model and the Wenzel model[4−8] were developed to calculate the contact angle on different substrates, according to which the relative magnitude of the surface tension between the substrate and the liquid determines the wettability of the surface. The roughness structure further enhances that wettability, for example, a hydrophobic surface will become superhydrophobic, while a hydrophilic surface will become superhydrophilic. Surfaces that are extremely repellant against water have special properties that give rise to potential applications in many fields. For example, corrosion[9,10] is normally caused by the oxidation of metal by oxygen dissolved in water, the diffusion of which can be prevented by making the surface or coating superhydrophobic and thus preventing the corrosion process. Most superhydrophobic materials have a self-cleaning effect,[11−14] in which the water droplet, while rolling off, automatically takes away dust on the material's surface. There have been a number of techniques developed for the fabrication of superhydrophobic surface. Chemical etching is commonly used on metal surfaces where etching processes provide surfaces with microscale roughness structure. Zhang et al.[15] has reported a highly robust superhydrophobic surface by using HCl to chemically etch aluminum alloy substrates followed by spraying coating of hydrophobic nanoparticles. Electrodeposition has also gained a lot of attention from many researchers because of its flexibility by controlling the applied voltage. De Leon et al.[16] has fabricated a superhydrophobic coating on stainless steel by combined colloidal templation and electropolymerization of a thiophene-derivative. The hierarchically structured polythiophene coating along with its redox capability gave the stainless steel substrate with superhydrophobicity and excellent corrosion protection.

Both superhydrophobicity and superoleophilicity can be imparted simultaneously by controlling the surface tension and the roughness of the substrate.[4−8] These surfaces have potential applications in separating oil from water.[17−20] Water is blocked, while oil can easily pass through the mesh with superhydrophobic and superoleophilic coating. Separation of oil from water is greatly valuable in the oil and gas industry for gasoline production and as a solution for cleaning oil spills, to name a few. Several techniques, including floatation, coagulation, biological treatment, and membrane separation technology, have been developed to treat oily wastewater. However, complex, multistep procedures, expensive processing cost, low separation efficiency, and secondary pollution still remain problems with these techniques.[21,22] Therefore, a superhydrophobic and superolephilic surface gained huge interest due to its easy production procedures, low cost, high efficiency, and absence of secondary pollution. Several techniques have been used to fabricate superhydrophobic and superoleophilic membranes for oil and water separation. Zhang et al.[23] reported a phase-inversion process where ammonia–water was added as

Received: June 5, 2015
Accepted: August 3, 2015
Published: August 3, 2015

DOI: 10.1021/acsami.5b04980
ACS Appl. Mater. Interfaces 2015, 7, 18566–18573

Scheme 1. Schematic of Spraying Coating of Thiol−ene Resin Followed by UV Curing to Fabricate Superhydrophobic/Superolephilic Mesh

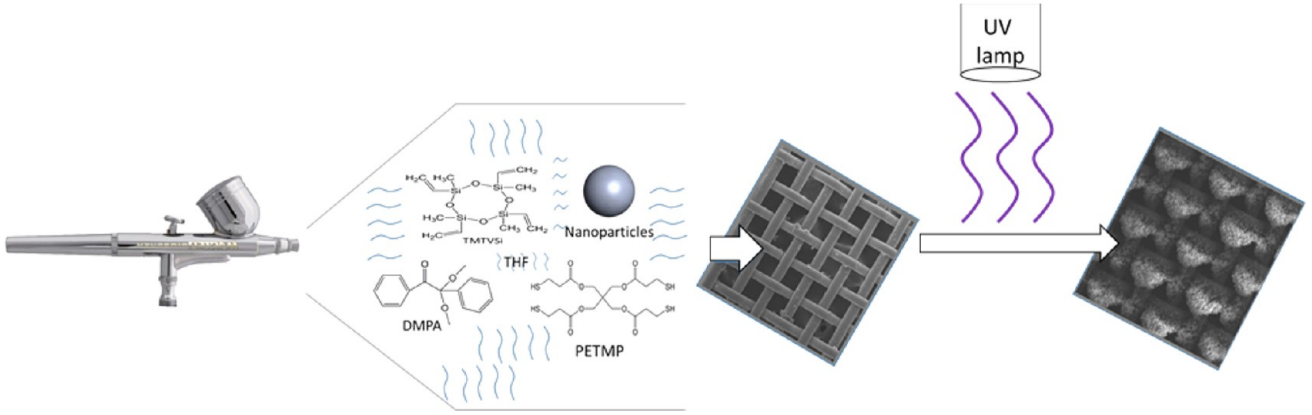

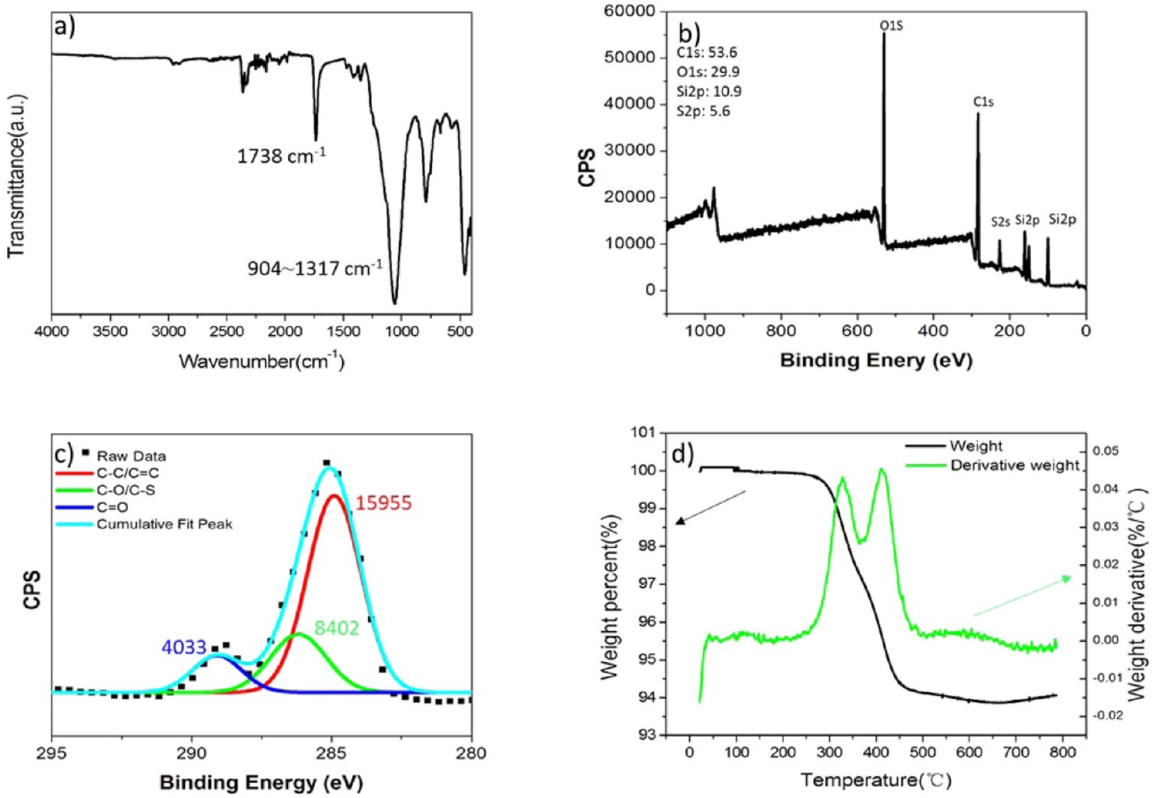

Figure 1. Coating characterization: (a) IR spectra, (b) XPS survey, (c) XPS high-resolution carbon scan, and (d) TGA analysis of the cured film.

an inert solvent additive into the PVDF solution successfully fabricated a water/oil separating membrane. Lee et al.[24] prepared a polystyrene nanofiber membrane by electrospinning electrically conductive polystyrene solution with nitric acid. Tang et al.[25] reported an in situ polymerized nanofibrous membrane by dip coating of 2,2-bis(3-octadecyl-3,4-dihydro-2*H*-1,3-benzoxazinyl)hexafluoro propane and SiO_2 NP solutions onto as-spun poly(m-phenylene isophthalamide) membrane, followed by polymerization at 200 °C. However, these technique all involved complex procedures and difficult experimental conditions. Spray coating, on the other hand, offers a number of advantages because of its applicability on various substrates, ease, and simplicity.[26−28] Nanoparticles can be dispersed in a polymer matrix and sprayed on the substrate to fabricate superhydrophobic films with good robustness, chemical resistance, and thermal stability.

Here, we report a facile two-step coating procedure, which involves spray coating of inorganic−organic thiol−ene with hydrophobic silica nanoparticles[29,30] on stainless mesh followed by photopolymerization. The coated stainless steel mesh was studied for its wetting property and its applicability for oil/water separation. The high efficiency of chain transfer reaction and oxygen resistance of the resulting resins[29,30] offer thiol−ene chemistry with highly rapid and ambient-condition reaction process. Superhydrophobicity/superolephilicity, water/oil separation efficiency, chemical resistance, thermal stability, and robustness of the coating on meshes with different aperture openings were studied.

DOI: 10.1021/acsami.5b04980
ACS Appl. Mater. Interfaces 2015, 7, 18566−18573

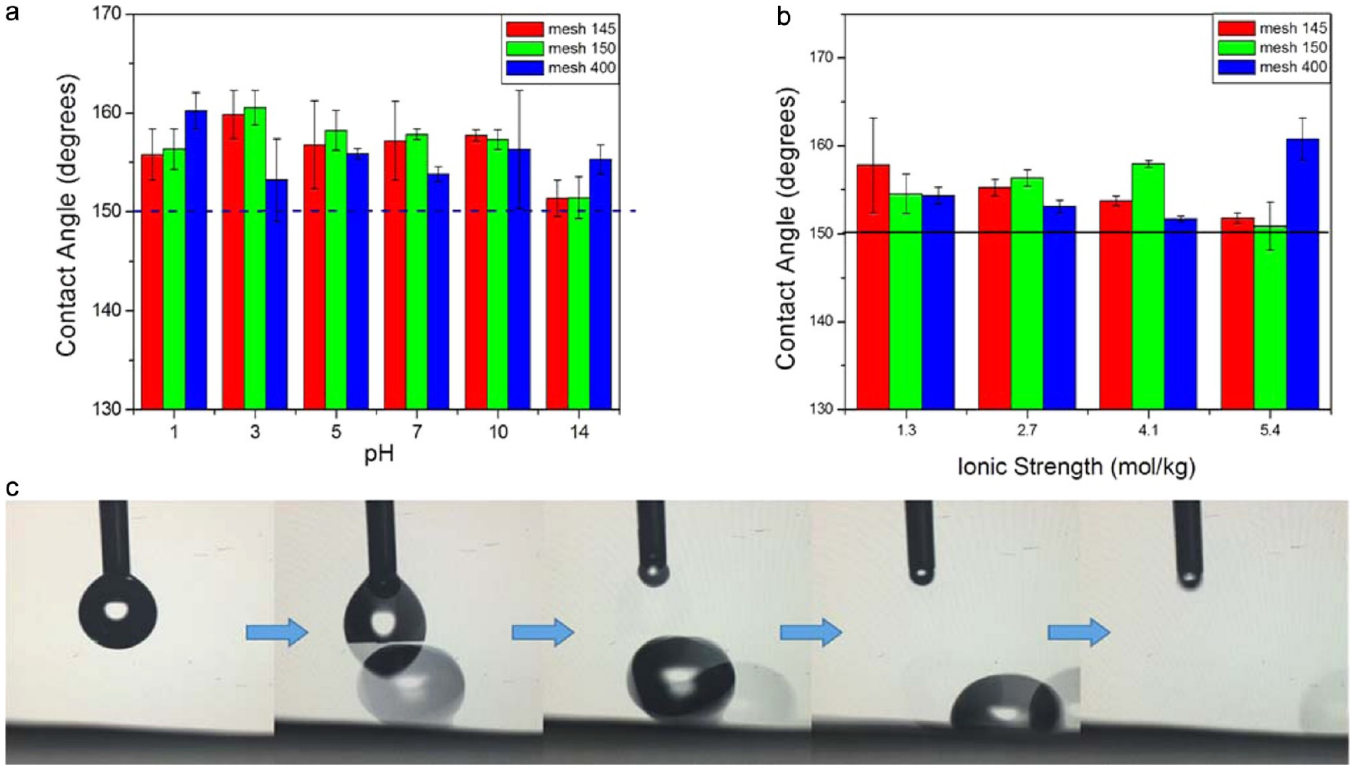

Figure 2. (a) Contact angles of water with different PH value on three different meshes. (b) Contact angles of water with different ionic strength on three different meshes. (c) Pictures of water bouncing off when dropped on coated mesh.

RESULTS AND DISCUSSION

We used a simple two-step approach to coat low surface energy film with multiscale roughness onto a stainless mesh (Scheme 1). The coating solution consists of pentaerythritol tetra(3-mercaptopropionate) (PETMP), 2,4,6,8-tetramethyl-2,4,6,8-tetravinylcyclotetrasiloxane (TMTVSi), and 2,2-dimethoxy-2-phenylacetophenone (DMPA), hydrophobic silica nanoparticles, all dissolved in tetrahydrofuran (THF). The coating solution was first spray-coated onto stainless mesh and then was exposed to UV light for curing. Photopolymerization took place during UV light curing[31,32] which forms a superhydrophobic/superoleophilic film with good thermal stability and chemical resistance.

Before curing, the absorbance of UV light wavelength range of uncured resin is required which have been characterized by conducting UV−vis spectrum. In Figure S1, UV−vis spectra of the uncured solution shows two absorbance peak at 245 and 350 nm. The former is due to the $\pi-\pi^*$ transition of the initiator, while the latter activates the Norrish type I α-cleavage reaction and produces benzoyl radical,[33−35] which initiates the reaction shown in Scheme S1.[36−38] Thus, light with a wavelength of 350 nm was used to cure the superhydrophobic coating.

After the UV light exposure, FT-IR spectroscopy was performed to characterize the functional groups present in the coating before and after curing and to check if the coating has been successfully cured. The IR spectra of cured film and pure PETMP, TMTVi, DMPA, and silica nanoparticles are shown in Figure 1a and Figure S2a. The broad peak in the range of 904−1317 cm^{-1} (Figure S2a,c) corresponds to Si−O−Si symmetric bond, and the peaks at 3067, 1600 cm^{-1} (Figure S2a) and 2566 cm^{-1} (Figure S2b) corresponds to the stretching of ═C−H bond, stretching of C═C bond of TMTVi, and thiol group of PETMP, respectively.[39−42] In addition, the peaks at 1738 cm^{-1} (Figure 1a and Figure S2b,d) correspond to C═O stretching bond. In Figure 1a, the corresponding peak in the range of 904−1317 cm^{-1} confirms the incorporation of silica nanoparticles in the cured film. On the other hand, the disappearance of the peaks at 3067, 1600, and 2566 cm^{-1} implies the reaction between C═C bond and thiol group, proving the success of the photopolymerization. To further confirm the result of IR spectra, XPS spectrum of cured film was also perfromed. As shown in Figure 1b, peaks at 100.4, 151.2, 162, and 283 eV coressponds to Si 2p and Si 2s of siloxane and S 2p, C 1s in C═O bond, respectively.[41−43] Peak areas indicate the relative amount of the specific elements at the surface of coated mesh. The relative area of each peak is also shown in Figure 1b. It can be calculated that the ratio of carbon to silica on the mesh surface is 1:0.2. The carbon to silica in the solution is 1:0.2816. The difference implies that there are more organic coatings on the surface and there are more silica nanoparticles underneath. Calculation based on molar mass and ratio of each components indicates that 43.15% of the loaded nanoparticles are on the surface. The high-resolution carbon scan is presented in Figure 1c where three deconvoluted carbon peaks can be observed. The integrated areas are shown beside each deconvoluted peaks. It is clearly seen that the area of the peak centered at 286.4 eV, which corresponds to both C−O bond and C−S bond, is twice that of the peak centered at 288.5 eV, which corresponds to the C═O bond. This is consistent with the structure of PETMP in which the ratio of the C−O, C−S, and C═O is 1:1:1. From the discussions above, we can conclude that films have been successfully cured on the stainless mesh after exposure to UV light.

The thermal property of the cured film on the stainless mesh is of interest because it determines the maximum working

DOI: 10.1021/acsami.5b04980
ACS Appl. Mater. Interfaces 2015, 7, 18566−18573

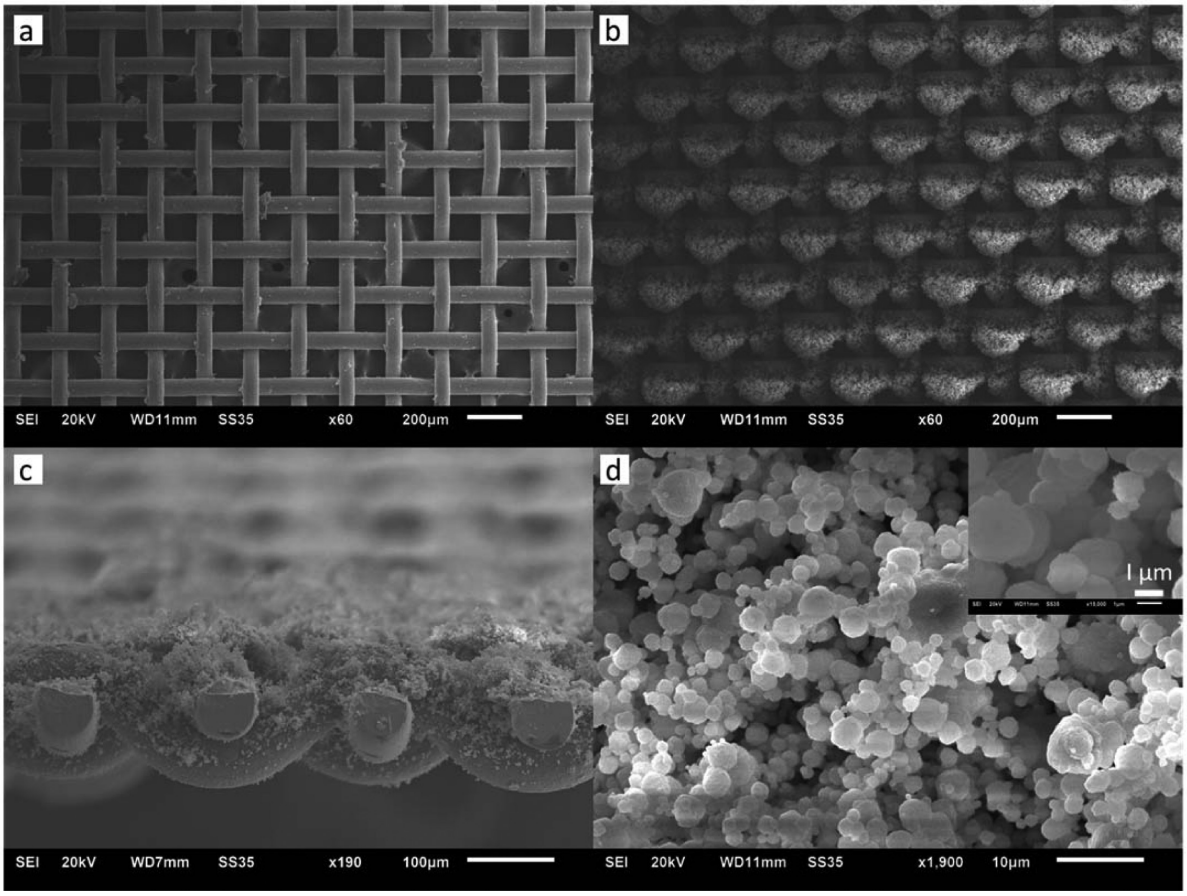

Figure 3. SEM images of mesh with 150 mesh number. (a) SEM image of uncoated mesh. (b) SEM image of coated mesh. (c) Cross section of coated mesh. (d) High magnification of coated mesh.

temperature that the coated mesh can be used. Thermogravimetric analysis was utilized and the thermogram is shown in Figure 1d. It can be seen from the weight percentage curve that the coated mesh is composed of 6 wt % polymer coating. Peaks at 327 and 411 °C can be seen in the weight derivative curve, which represent two degradation temperatures of superhydrophobic coating. These two degradation temperatures correspond to the breaking of the (1) C−C bond and Si−C and (2) C−H cleavage, respectively.[44] Also, the absence of any peaks below 200 °C, signifies that there are no water and low boiling point components (THF solvent) incorporated in the polymer matrix. The results of the thermogravimetric analysis shows that the mesh is usable until 300 °C, which has been further confirmed by measuring water contact angles, as shown in Table S1, after keeping meshes at 300 °C for 50 min. This outstanding thermal stability can be explained by the fact that the cured film has high degree of cross-linking.

To demonstrate that coated meshes are superhydrophobic, which is essential for water/oil separation, and to demonstrate that meshes have good chemical resistance so that they can be applied in various environments, we have conducted experiments of complete immersion of the coated meshes in solutions of pH 1−14 and of different ionic strengths for 30 min followed by contact angle using pure, neutral water as the probe. The measured contact angles are shown in Figure 2a,b. It can be seen that after complete immersion in different water conditions for 30 min, all contact angles remain higher than 150°, indicating that films have very good resistance to strong acid, base, and electrolyte. In Figure 2c, it is shown that droplets can easily roll off when dropped onto a coated mesh with a slope of less than 3°, further proving that droplets are strongly repelled by the coated mesh. The repelling phenomena can be explained by the Cassie−Baxtel state due to the multiscale roughness structure of the coated hybrid films, which are shown in the scanning electron microscopy (SEM) images in Figure 3. The rough structure provides meshes with enough trapped air at the surface around the nanoparticle aggregates. The dropped water cannot penetrate the trapped air and is thus repelled. This rolling-off behavior of dropped water gives rise to the self-cleaning capability of the coated mesh. Dust and dirt on the mesh can be automatically taken away by a water droplet when it rolls off the mesh. To further confirm the self-cleaning effect, a demonstration experiment is conducted and shown in Figure S4.

The surface morphology of the coated stainless steel mesh was investigated by SEM. Figure 3 shows the SEM images of the coated and the uncoated mesh. The SEM image of the uncoated bare mesh (Figure 3a) shows a very smooth surface and evenly arranged mesh wires across whole surface, while the SEM image of the coated mesh (Figure 3b) displays a uniformly coated films with evident rough surface covering the whole mesh wires. The cross-sectional image in Figure 3c shows that the mesh is coated thoroughly onto the top of mesh wires and partially on the top half of the sidewalls of mesh wires. Multiscale surface roughness can be seen in Figure 3d, where microscale roughness structure is possibly derived from fast evaporation of THF during spraying which left pores in the resin film while the agglomeration of silica nanoparticles

DOI: 10.1021/acsami.5b04980
ACS Appl. Mater. Interfaces 2015, 7, 18566−18573

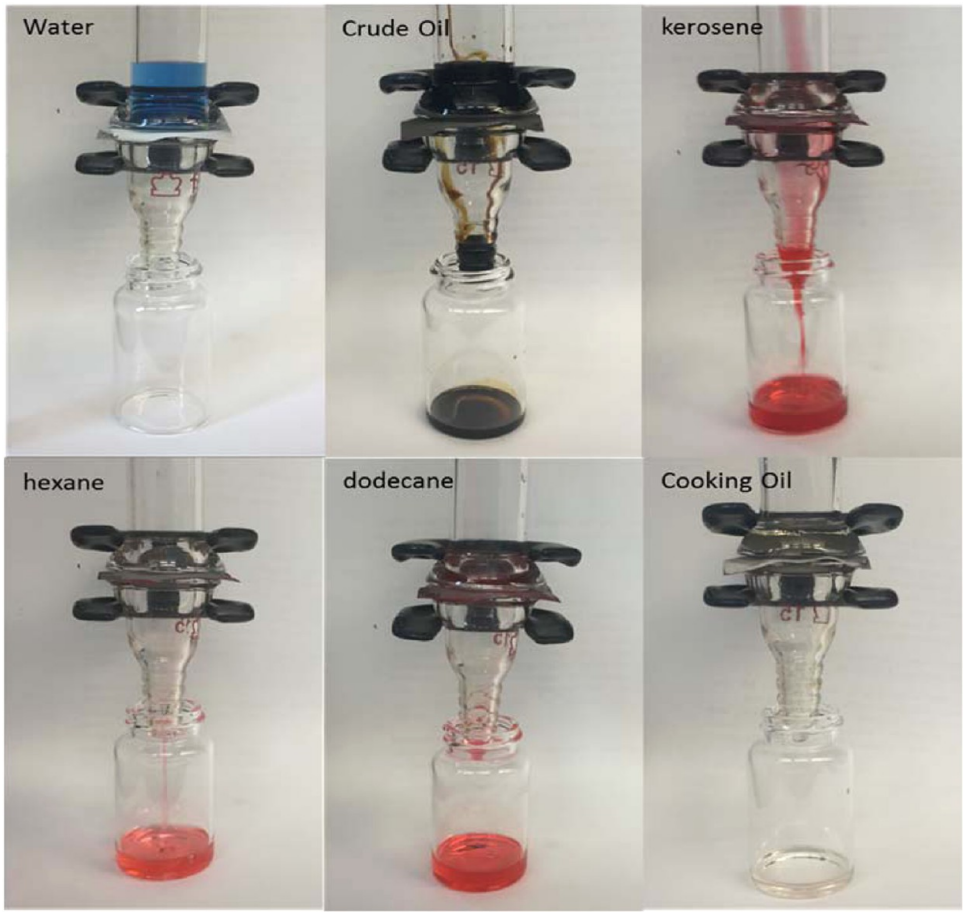

Figure 4. Optical images of water on and five different oil passing through the superhydrophobic-coated mesh.

dispersed at the resin film surface provides the micro- and nanoscale roughness.[15] The multiscale roughness structure is further solidified in the following UV curing process and gives rise to superhydrophobic wetting behavior demonstrated in Figure 2.

For the realization of water/oil separation effect, the superhydrophobicity acts as the closed gate to block water, superolephilicity is also required to act as open gate for oil to smoothly penetrate the mesh. To demonstrate the superolephilicity, five different oils—dodecane, hexane, cooking oil, kerosene, and crude oil—were chosen to test the oil wettability of the coated mesh. All the tested oils showed superoleophilicity, characterized by 0° oil contact angle. It can be seen in Figure 4 that the water droplet (dyed blue for clarity) remained on the mesh while oil droplets (some are dyed red) easily pass through the mesh, which indicates the superolephilicity of the mesh. After photopolymerization, the surface energy of the films is lower than that of water but higher than that of oil.[45] The wetting behavior of different oils on mesh is characteristic of Wenzel wetting state[6] that the positive difference of mesh surface energy to that of oil will result in the oil wetting the surface.

Due to the simultaneous superhydrophobicity and superolephilicity of the film, coated meshes can be used to separate oil and water. Therefore, we measured the separation efficiency of five different oils (the same as above) from water by using different prepared meshes, and results are shown in Figure 5. Mesh was tested in separating the oil from water. The oil and water was first mixed to form a bilayer before being introduced on the coated mesh. The oil that passed through was collected, and an equal volume of acetonitrile (ACN) was added to it. Only water, and not the oil, is miscible in acetonitrile. An infrared spectrum of the ACN, now with the water, was taken after the ACN and oil layers were completely separated. The water/dodecane separation efficiency is shown in Figure 5, and the results of the other oils are shown in Figure S3.

The calibration plot of dodecane/water system was prepared by taking the IR spectra of acetonitrile (ACN) mixed with dodecane that contains 0.1, 1, 2, 3, 4, and 5 vol % of water (shown in Figure 5a) . The calibration plots for other oils are presented in Figure S3. The spectrum of the ACN mixed with oil that contains no water was used as the background. The peak between 3200 and 3700 cm^{-1} corresponds to the O−H stretching of the water molecule. Ploting the transmittance at 3600 cm^{-1} against the concentration of water shows a linear trend, as shown in Figure 5b. By fitting the transmittance at 3600 cm^{-1} of the ACN added to the oil that passed through the mesh in the calibration curve, separation efficiency results can be calculated. As shown in Figure 5c, it is clear that meshes with different mesh number all have separation efficiency higher than 99.85% for the five tested oils. When the concentration of water in ACN is smaller than 0.2% (separation efficiency higher than 99.8%), the FTIR curve is almost flat, and the noise is in the same magnitude with peak at 3600 cm^{-1}. But the calibration curve is very linear, which makes it appropriate in estimating the separation efficiency. There is no trend of efficiency change with different mesh numbers. The absence of trend partially attributes to the noise but most likely is because

DOI: 10.1021/acsami.5b04980
ACS Appl. Mater. Interfaces 2015, 7, 18566−18573

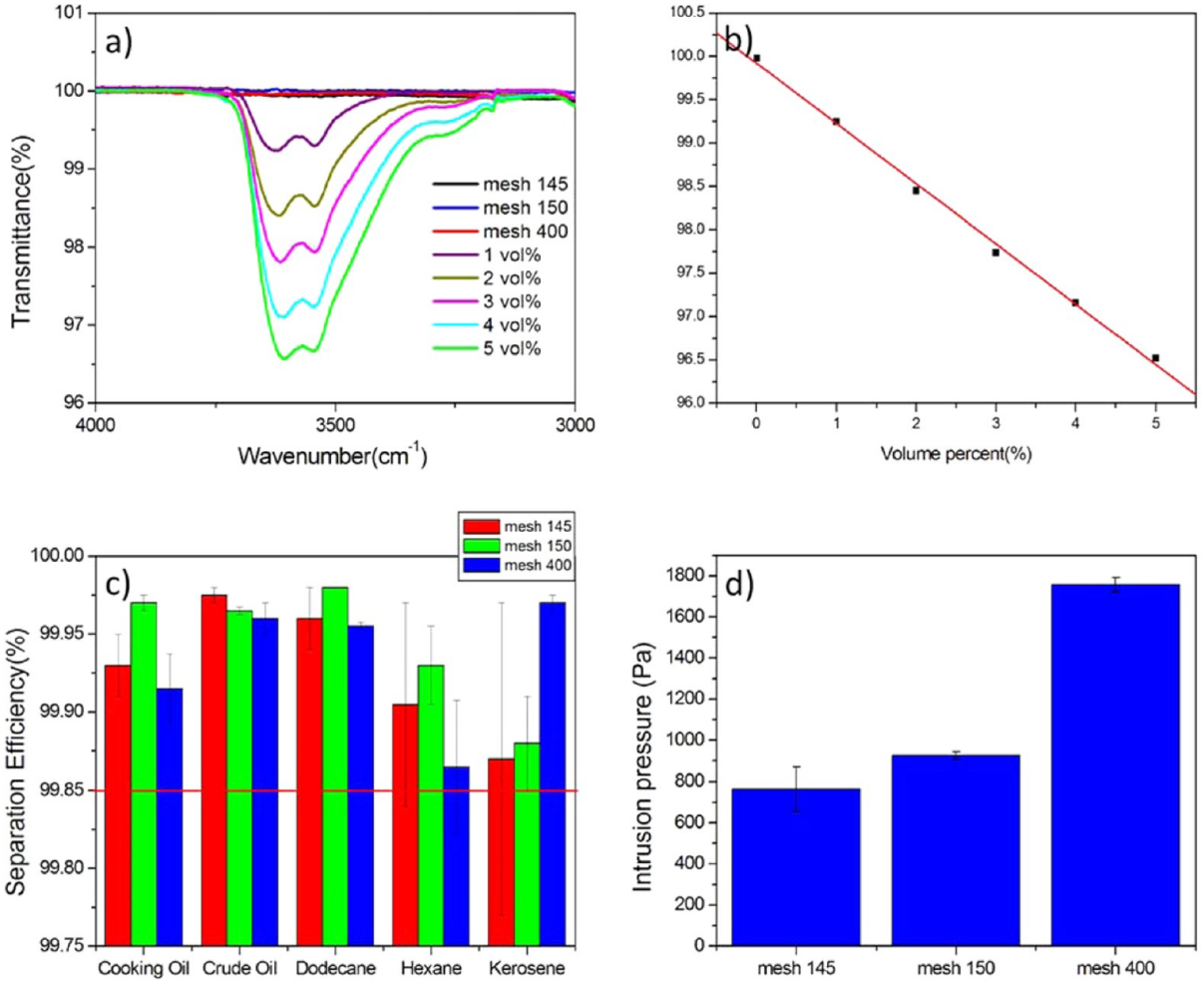

Figure 5. (a) IR spectrum of water/dodecane separation product in ACN and water with different concentration in ACN. (b) Calibration curve of IR spectrum for different water concentrations in ACN. (c) Separation efficiency of five chosen oils of meshes with different mesh number. (d) Intrusion pressure of water for meshes with different mesh number.

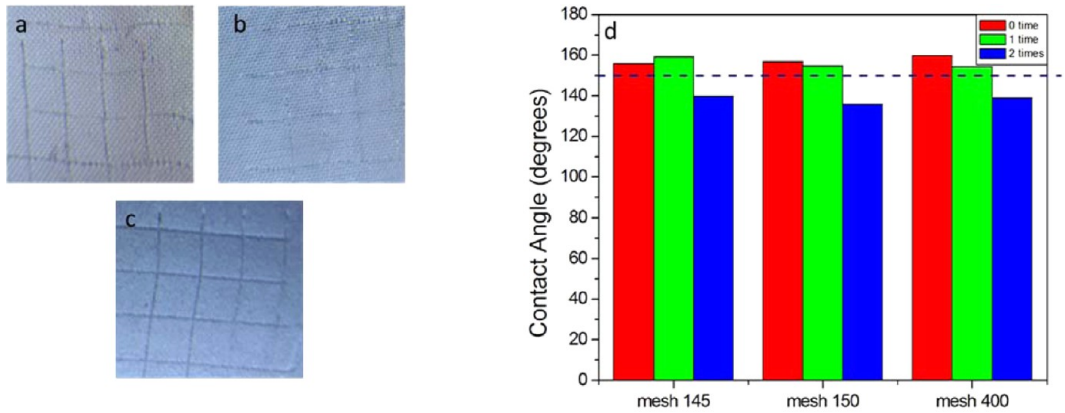

Figure 6. Mechanical testing results of three different coated meshes based on ASTM standard testing. (a–c) Digital photographs of one-time peeling result after the formation of cross-cut grid cross sections of mesh 145, mesh 150, and mesh 400, respectively. (d) water contact angle results of three different meshes after 2 times peeling.

the films with different mesh numbers all have reached the limit of efficiency for the film since it is nearly 100%. Besides, the fact that noise can be the same magnitutude with identification peak indicates that the separation efficiency is already higher than 99.8%, above which the trend of efficiency makes no significant sense.

For separation applications in large scale production, coated meshes are required to stand large amount of mix liquid without water penetrating through meshes. This liquid-holding capacity can be characterized by intrusion pressure. It is measured by continuously adding water on meshes until water pressure reaches a threshold, in which water starts penetrating

DOI: 10.1021/acsami.5b04980
ACS Appl. Mater. Interfaces 2015, 7, 18566–18573

the meshes. As shown in Figure 5d, intrusion pressure increases as the mesh number increases. This is due to the decrease of areas of openings in the meshes as mesh number increases. For mesh 145, intrusion pressure reaches 0.764 kPa, while for mesh 400, intrusion pressure reaches 1.758 kPa. The adhesion strength has also been studied because good adhesion strength is desired to prevent possible scratches and liquid flowing forces to damage surface structure. The coated meshes are cut by sharp razor blade to form cross-cut grid cross sections, followed by tight tape adhesion covering the grid cross sections for 60 s. Results of one-time peeling of coatings after removal of the tape are shown in Figure 6a–c, corresponding to mesh 145, mesh 150, and mesh 400, respectively. According to ASTM D3359-09$^{\varepsilon 2}$, coated films on all the meshes have classification of adhesion test better than 4B (less than 5% removed), which reveals excellent adhesion strength. Contact angles have been measured for meshes with different mesh number after the peeling of coated films by applying tape adhesion for 60 s for multiple times. After one-time peeling, as shown in Figure 6d, contact angles of water on coated films of all meshes are above 150 °, which demonstrated that coated films still maintain superhydrophobicity, further proving the excellent adhesion strength of the coating. The fact that the mesh can hold significant water pressure without failing and high resistance of peeling by tape demonstrates that the coated mesh is very robust and very stable. The cross-linking reaction during UV curing solidifies the film that improves the attachment of film on mesh wires and stabilizes nanoparticles dispersed at the surface of the film. Thus, the high solidification curing process provides film with good robustness. Excellent superhydrophobicity and superolephilicity of the mesh are key factors for excellent separation efficiency. Superhydrophobicity works to block the water, while superolephilicity works as the open gate of oil. In addition, good robustness is also required to prevent nanoparticles on the films flushed away, as well to prevent the multiscale roughness structure damaged while oil penetrates the mesh.

CONCLUSION

In conclusion, we have successfully fabricated a superhydrophobic/superoleophilic mesh with multiscale roughness structure by a simple two-step approach of spray coating followed by UV curing. This mesh demonstrates excellent thermal stability and chemical resistance, with degradation temperature as high as 327 °C and maintanance of superhydrophobicity under strong acid, base, and ionic strength. The multiscale roughness structure results in Cassie–Baxter state on the mesh that enough air is trapped at the surface to repel water. The thiol–ene chemistry leads to cross-linked structure after UV curing which offers excellent thermal stability and chemical resistance. In addition, highly cross-linked structure largely increased the intrusion pressure and adhesion strength, revealing excellent mechanical property of coated film. Water/oil separation efficiency reaches up to more than 99.85% which results from the combination of excellent superhydrophobicity and mechanical strength.

EXPERIMENTAL SECTION

Materials. Chemical reagents were used without further purification unless otherwise specified. 2,4,6,8-Tetramethyl-2,4,6,8-tetravinylcyclotetrasiloxane (TMTVSi), 2,2-dimethoxy-2-phenylacetophenone (DMPA), and pentaerythritol tetra(3-mercaptopropionate) (PETMP) were obtained from Sigma-Aldrich. Aerosil R812S, hydrophobic fumed silica aftertreated with HMDS based on AEROSIL 300, was kindly provided by Evonik Corporation (Mobile, AL).

Characterization. UV–vis spectra were obtained on an Agilent 8453 spectrometer. Scan electron microscopy analysis was measured using FEI XL-30FEG SEM equipped with Nanopattern Generation System. Static water contact angle was done using a CAM 200 optical contact angle meter. FTIR spectroscopy measurements was done with Digilab FTS 7000 ATR rapid scan spectrometer in transmittance mode. XPS data was acquired using a Physical Electronics 5700 X-ray Photoelectron Spectrometer with a monochromatic Al Kr irradiation X-ray source ($h\nu$ = 1486.7 eV). Photoelectrons were collected at takeoff angle of 45° from the surface with a hemispherical energy analyzer. Thermogravimetric analysis were recorded on TA Instruments, TGA 2950. Coated meshes were heated up to 800 °C with a heating rate of 15 °C/min.

Coating Preparation. Coating solutions were prepared by combining TMTVSi and PETMP with stoichiometric ratio of 1:1 as the thiol–ene resin, along with DMPA as the photo initiator (0.005:1 w/w initiator/resin) and hydrophobic silica nanoparticles (Aerosil R812S; 0.3:1 w/w nanoparticles/resin) to be dispersed in THF (15:1 w/w solvent/resin) and then by ultrasonication for 15 min. Stainless meshes with mesh numbers 145, 150, and 400 were precleaned in acetone by sonication for 5 min. As-prepared solution was spray coated onto precleaned meshes by an airbrush connected to an air compressor. The coated meshes were cured under UV lamp (20 mW/m^2) for 5 min and were subsequently dried in the oven at 60 °C for 30 min to completely remove the THF residue.

ASSOCIATED CONTENT

Supporting Information

The Supporting Information is available free of charge on the ACS Publications website at DOI: 10.1021/acsami.5b04980.

UV–vis spectrum of the uncured thiol–ene solution; FTIR spectrum of individual resin components TMTVSi, PETMP, hydrophobic silica nanoparticles (Aerosil 812S), DMPA; mechanism of initiating process of DMPA.; IR spectrum of water/oil separation product in ACN and water with different concentration in ACN; calibration curves of IR spectra for different water concentraions in ACN: cooking oil, hexane, kerosene, and crude oil; demonstration experiment of self-cleaning effect; contact angles of meshes with different mesh numbers after being kept at 300 °C for 50 min. (PDF)

AUTHOR INFORMATION

Corresponding Author

*E-mail: rca41@case.edu. Phone: +1 216-368-4566.

Notes

The authors declare no competing financial interest.

ACKNOWLEDGMENTS

We gratefully acknowledge funding from DMR-1304214 and technical support from Malvern (Viskotek), Biolin, Agilent Technologies, and Park Systems.

REFERENCES

(1) Cheng, Y. T.; Rodak, D. E. Is the Lotus Leaf Superhydrophobic? *Appl. Phys. Lett.* **2005**, *86* (14), 4101.

(2) Barthlott, W.; Neinhuis, C. Purity of the Sacred Lotus, or Escape from Contamination in Biological Surfaces. *Planta* **1997**, *202* (1), 1–8.

(3) Neinhuis, C.; Barthlott, W. Characterization and Distribution of Water-repellent, Self-cleaning Plant Surfaces. *Ann. Bot.* **1997**, *79* (6), 667–677.

(4) Marmur, A. Wetting of Hydrophobic Rough Surfaces: To be Heterogeneous or not to be. *Langmuir* **2003**, *19* (20), 8343–8348.

DOI: 10.1021/acsami.5b04980
ACS Appl. Mater. Interfaces 2015, 7, 18566–18573

(5) Lafuma, A.; Quere, D. Superhydrophobic States. *Nat. Mater.* **2003**, *2* (7), 457−8348.
(6) Wenzel, R. N. Resistance of Solid Surfaces to Wetting by Water. *Ind. Eng. Chem.* **1936**, *28* (8), 988−994.
(7) Cassie, A. B. D.; Baxter, S. Wettability of Porous Surfaces. *Trans. Faraday Soc.* **1944**, *40*, 546−551.
(8) Onda, T.; Shibuichi, S.; Satoh, N.; Tsujii, K. Super-Water-Repellent Fractal Surfaces. *Langmuir* **1996**, *12* (9), 2125−2127.
(9) Jacobs, J. J.; Gilbert, J.; Urban, R. Corrosion of Metal Orthopaedic Implants. *J. Bone Joint Surg. Am.* **1998**, *80* (2), 268−282.
(10) De Leon, A.; Pernites, R.; Advincula, R. Superhydrophobic Colloidally Textured Polythiophene Film as Superior Anticorrosion Coating. *ACS Appl. Mater. Interfaces* **2012**, *4* (6), 3169−3176.
(11) Fürstner, R.; Barthlott, W.; Neinhuis, C.; Walzel, P. Wetting and Self-Cleaning Properties of Artificial Superhydrophobic Surfaces. *Langmuir* **2005**, *21* (3), 956−961.
(12) Blossey, R. Self-Cleaning Surfaces-Virtual Realities. *Nat. Mater.* **2003**, *2*, 301−306.
(13) Wagner, P.; Fürstner, R.; Barthlott, W.; Neinhuis, C. Quantitative Assessment to the Structural Basis of Water Repellency in Natural and Technical Surfaces. *Journal of Experimental Botany J. exp. Bot.* **2003**, *54* (385), 1295−1303.
(14) Nakajima, A.; Hashimoto, K.; Watanabe, T.; Takai, K.; Yamauchi, G.; Fujishima, A. Transparent Superhydrophobic Thin Films with Self-Cleaning Properties. *Langmuir* **2000**, *16* (17), 7044−7047.
(15) Zhang, Y. F.; Ge, D. T.; Yang, S. Spray-Coating of Superhydrophobic Aluminum Alloys with Enhanced Mechanical Robustness. *J. Colloid Interface Sci.* **2014**, *423*, 101−107.
(16) De Leon, A.; Pernites, R.; Advincula, R. Superhydrophobic Colloidally Textured Polythiophene Film as Superior Anticorrosion Coating. *ACS Appl. Mater. Interfaces* **2012**, *4* (6), 3169−3176.
(17) Chen, P.-C.; Xu, Z.-K. Mineral-Coated Polymer Membranes with Superhydrophilicity and Underwater Superoleophobicity for Effective Oil/Water Separation. *Sci. Rep.* **2013**, *3*, 2776.
(18) Solomon, B. R.; Hyder, M. N.; Varanasi, K. K. Separating Oil-Water Nanoemulsions Using Flux-Enhanced Hierarchical Membranes. *Sci. Rep.* **2014**, *4*, 5504.
(19) Lee, C.; Johnson, N.; Drelich, J.; Yap, Y. The Performance of Superhydrophobic and Superoleophilic Carbon Nanotube Meshes in Wate-Oil Filtration. *Carbon* **2011**, *49* (2), 669−676.
(20) Tian, D.; Zhang, X.; Tian, Y.; Wu, Y.; Wang, X. Photo-Induced Water−Oil Separation Based on Switchable Superhydrophobicity Superhydrophilicity and Underwater Superoleophobicity of the Aligned ZnO Nanorod Array-Coated Mesh Films. *J. Mater. Chem.* **2012**, *22* (37), 19652−19657.
(21) Coca, J; Gutiérrez, G. *Water Purification and Management*. Springer: New York, 2011.
(22) Yu, L.; Han, M.; He, F. A Review of Treating Oily Wastewater. *Arabian J. Chem.* **2013**, DOI: 10.1016/j.arabjc.2013.07.020.
(23) Zhang, W. B.; Shi, Z.; Zhang, F.; Liu, X.; Jin, J.; Jiang, L. Superhydrophobic and Superoleophilic PVDF Membranes for Effective Separation of Water-in-oil Emulsions with High Flux. *Adv. Mater.* **2013**, *25*, 2071−2076.
(24) Lee, M. W.; An, S.; Latthe, S. S.; Lee, C.; Hong, S.; Yoon, S. S. Electrospun Polystyrene Nanofiber Membrane with Superhydrophobicity and Superoleophilicity for Selective Separation of Water and Low Viscous Oil. *ACS Appl. Mater. Interfaces* **2013**, *5*, 10597.
(25) Tang, X.; Si, Y.; Ge, J.; Ding, B.; Liu, L.; Zheng, G.; Luo, W.; Yu, J. In Situ Polymerized Superhydrophobic and Superoleophilic Nanofibrous Membranes for Gravity Driven Oil−Water Separation. *Nanoscale* **2013**, *5*, 11657.
(26) Feng, L.; Zhang, Z.; Mai, Z.; Ma, Y.; Liu, B.; Jiang, L.; Zhu, D. A Super-Hydrophobic and Super-Oleophilic Coating Mesh Film for the Separation of Oil and Wate. *Angew. Chem., Int. Ed.* **2004**, *43*, 2012.
(27) Levkin, P. A.; Svec, F.; Frechet, J. M. J. Porous Polymer Coatings: a Versatile Approach to Superhydrophobic Surfaces. *Adv. Funct. Mater.* **2009**, *19* (12), 1993−1998.
(28) Manoudis, P. N.; Karapanagiotis, I.; Tsakalof, A.; Zuburtikudis, I.; Panayiotou, C. Superhydrophobic Composite Films Produced on Various Substrates. *Langmuir* **2008**, *24* (19), 11225−11232.
(29) Sparks, B. J.; Hoff, E. F. T.; Xiong, L.; Goetz, J. T.; Patton, D. T. Superhydrophobic Hybrid Inorganic−Organic Thiol-ene Surfaces Fabricated via Spray-Deposition and Photopolymerization. *ACS Appl. Mater. Interfaces* **2013**, *5* (5), 1811−1817.
(30) Schwalm, R. *UV Coatings: Basics, Recent Developments and New Applications*. Elsevier: Amsterdam, 2007.
(31) Hoyle, C. E.; Bowman, C. N. Thiol−Ene Click Chemistry. *Angew. Chem., Int. Ed.* **2010**, *49* (9), 1540−1573.
(32) Hoyle, C. E.; Lee, T. Y.; Roper, T. J. Thiol−Enes: Chemistry of the Past with Promise for the Future. *J. Polym. Sci., Part A: Polym. Chem.* **2004**, *42* (21), 5301−5338.
(33) Taranekar, P.; Park, J. Y.; Patton, D.; Fulghum, T.; Advincula, R. Conjugated Polymer Nanoparticles via Intramolecular Crosslinking of Dendrimeric Precursors. *Adv. Mater.* **2006**, *18* (18), 2461.
(34) Cao, P.; Felipe, M.; Advincula, R. On the Formation and Electropolymerization of a Star Copolymer With Peripheral Carbazoles. *Macromol. Chem. Phys.* **2013**, *214* (3), 386−395.
(35) Segurola, J.; Allen, N.; Edge, M.; Roberts, J. Photochemistry and Photoinduced Chemical Crosslinking Activity of Acrylated Prepolymers by Several Commercial Type I Far UV Photoinitiators. *Polym. Degrad. Stab.* **1999**, *65* (1), 153−160.
(36) Fischer, H.; Baer, R.; Hany, R.; Verhoolen, I.; Walbiner, M. 2,2-Dimethoxy-2-Phenylacetophenone: Photochemistry and Free Radical Photofragmentation. *J. Chem. Soc., Perkin Trans. 2* **1990**, *5*, 787−798.
(37) Fouassier, J. P.; Jacques, P.; Lougnot, D. J.; Pilot, T. Lasers, Photoinitiators and Monomers: a Fashionable Formulation. *Polym. Photochem.* **1984**, *5* (1−6), 57−76.
(38) Hageman, H. J. Photoinitiators for Free Radical Polymerization. *Prog. Org. Coat.* **1985**, *13* (2), 123−150.
(39) Smith, A. L. Infrared Spectra-Structure Correlations for Organosilicon Compounds. *Spectrochim. Acta* **1960**, *16* (1), 87−105.
(40) Coates, J. Interpretation of Infrared Spectra, A Practical Approach. In *Encyclopedia of Analytical Chemistry*; Meyers, R. A., Ed.; John Wiley & Sons, Ltd.: Chichester, 2000. pp 10815−10837.
(41) Pangilinan, K.; Santos, C.; Estillore, N.; Rodrigues, D.; Advincula, R. Temperature Responsiveness and Antimicrobial Properties of CNT/PNIPAM Hybrid Brush Films. *Macromol. Chem. Phys.* **2013**, *214* (4), 464−469.
(42) Zhou, Q.; Wang, S.; Fan, X.; Advincula, R.; Mays, J. Living Anionic SurfaceInitiated Polymerization (LASIP) of a Polymer on Silica Nanoparticle. *Langmuir* **2002**, *18*, 3324−3331.
(43) Erdem, B.; Hunsicker, R.; Simmons, G.; Sudol, E. D.; Dimonie, V.; El-Aasser, M. XPS and FTIR Surface Characterization of T_iO_2 Particles Used in Polymer Encapsulation. *Langmuir* **2001**, *17* (9), 2664−2669.
(44) Tyng, Y. L.; Ramli, M. R.; Othman, M. B. H.; Ramli, R.; Ishak, Z. A. M.; Ahmad, Z. Effect of Crosslink Density on the Refractive Index of a Polysiloxane Network Based on 2,4,6,8-Tetramethyl-2,4,6,8-Tetravinylcyclotetrasiloxane. *Polym. Int.* **2013**, *62* (3), 382−389.
(45) Zisman, W. A. Relation of the Equilibrium Contact Angle to Liquid and Solid Constitution In *Contact Angle, Wettability, and Adhesion*; Fowkes, F. M., Ed.; Advances in Chemistry Series 43; American Chemical Society: Washington, D.C., 1964; pp 1−51.

DOI: 10.1021/acsami.5b04980
ACS Appl. Mater. Interfaces 2015, 7, 18566−18573